Chinese Chemical Letters 31 (2020) 439–442

Contents lists available at ScienceDirect

Chinese Chemical Letters

journal homepage: www.elsevier.com/locate/cclet

Communication

Constructing boronate-bridged core-satellite gold nanoassembly and its application in high sensitive colorimetric detection of benzoyl peroxide residues in food matrices

Ting Li[a,b,1], Jiefang Sun[b,1], Jinyuan Liu[a,b], Baolei Dong[c], Huachao Zhao[d], Xiaoting Qiao[b], Wencong Shan[c], Jing Zhang[b], Bing Shao[a,b,*]

[a] School of Public Health, Capital Medical University, Beijing 100069, China
[b] Beijing Key Laboratory of Diagnostic and Traceability Technologies for Food Poisoning, Beijing Center for Disease Prevention and Control, Beijing 100013, China
[c] Beijing Advanced Innovation Center for Food Nutrition and Human Health, China Agricultural University, Beijing 100193, China
[d] College of Chemical Engineering and Materials Science, Tianjin University of Science and Technology, Tianjin 300457, China

ARTICLE INFO

Article history:
Received 27 May 2019
Received in revised form 26 August 2019
Accepted 27 August 2019
Available online 29 August 2019

Keywords:
Benzoyl peroxide
Colorimetric detection
Gold nanoassembly
Deboronation
Food safety

ABSTRACT

Here, a new designed core/satellite gold nanoprobe was developed for detecting trace mount of benzoyl peroxide (BPO) based on its deboronation. This gold nanoassembly (the BE-AuNPs$_{12/65}$) was constructed *via* borate ester formation between large 4-mercaptophenylboronic acid (MPBA) modified AuNPs (the MPBA-AuNPs$_{65}$, as cores) and small dopamine modified AuNPs (the DPA-AuNPs$_{12}$, as satellites). Particularly, upon addition of BPO, it would trigger the deboronation for the BE-AuNPs$_{12/65}$ probes accompanying with distinct color changes from blue, purple to wine red, which implied the disassembly of the core/satellite nanostructure after the breakage of carbon to boron chemical bond. By measuring the absorbance ratio at 665 nm and 545 nm, quantification of BPO was achieved in the range of 10.0–100.0 nmol/L, which could also be easily observed by naked eyes. The nanoprobe utilized a boronate deprotection mechanism and the LSPR properties of AuNPs to provide high selectivity for detecting BPO over similar ROS/RNS with the limit of detection as low as 7.2 nmol/L. The practical applicability of this assay was verified through successful determining BPO in flour samples, which demonstrated its great potentials in food safety field.

As a reactive oxygen species (ROS), benzoyl peroxide (BPO) had been once widely employed as flour additives to improve the color and luster [1], until the tissue damage of BPO for human body become the public concerns [2,3]. Because of these harmful effects, in 1997 it is no longer permitted to be used as flour additive by European Union. Until 2011, seven departments in China announced the ban of adding BPO into flour [4]. Even if BPO are currently banned in many countries, they could still potentially illegally used in foods. So far, many instrument based analytic methods have been developed for such kind of substance [5–7]. Although these methods could provide accurate and definite detecting results, strong dependence for sophisticated instruments restricted their uses in resource-limited areas. Until now, some optical organic probes have been designed for rapid optical detection for BPO in real samples [8,9]. But these chemo-sensors always entail sophisticated design, complicated synthesis and large consumption of harmful chemical reagents.

Over the past two decades, plasmonic nanomaterials based colorimetric assays, which took advantage of color changes that arises from the interparticle plasmon coupling have received considerable attentions for developing highly selective, prompt, low-cost and user-friendly nanosensors for a wide variety of targets [10–13]. Benefitting from their strong localized surface plasmon resonance (LSPR) extinctions in visible light regions, these nanoprobes could overcome low sensitivities and high costs involved in fabricating organic optical probes [14–16]. In this aspect, chemical reaction-assisted assembly/disassembly of nanostructures are of exciting controls over different surface functionalized nanoparticles, which could fabricate special signal readout platforms for a wide variety of sensing systems [17–22].

In this work, a core-satellite Au nanoassembly was proposed for direct, selective and high sensitive colorimetric detection of BPO based on its specific deboronation. Specifically, 4-mercaptophenylboronic acid (MPBA) was modified on the core AuNPs (~65 nm, the MPBA-AuNPs$_{65}$). On the other hand, a monolayer of thiolate acid (TA) was

* Corresponding author at: School of Public Health, Capital Medical University, Beijing 100069, China.
E-mail address: shaobingch@sina.com (B. Shao).
[1] These authors contributed equally to this work.

https://doi.org/10.1016/j.cclet.2019.08.051
1001-8417/

modified on the smaller Au NPs (~12 nm), and then covalently linked with dopamine (DPA) *via* amide linkage to obtain the DPA coated AuNPs (the DPA-AuNPs$_{12}$). As shown in Scheme 1, the specific esterification under weak base solution (pH 8.5) between the boronic acid in MPBA and diols in DPA could trigger the fabrication of the stable core-satellite Au nanoassemblies, and obtaining the target-specific nano-sensing interface. As the intermediate of BPO-triggered deboronation, the carbon to boron chemical bonds among the interparticle junctions of the BE-AuNPs$_{12/65}$ were broken, thus leading to distinct blue-shift of LSPR. By monitoring the absorbance ratio at 665 nm and 545 nm, a colorimetric assays for BPO was realized. The specific chemical recognition, together with the amplifying properties of plasmonic nanostructure, was important to enable their high sensitivity and selectivity.

Spherical AuNPs with different sizes were synthesized and characterized (Fig. S1 in Supporting information) according to previous reported method [23], and further modified with MPBA and DPA. The obtained DPA-AuNPs$_{12}$ and the MPBA-AuNPs$_{65}$ were assembled to form the BE-AuNPs$_{12/65}$ under weak basic condition. The detailed preparation for different modified AuNPs as well as subsequent assemble process can be found in Supporting information. After purification, the BE-AuNPs$_{12/65}$ was standardized to 1.3 OD at 665 nm using UV–vis spectroscopy. Various concentrations of BPO were added to the BE-AuNPs$_{12/65}$ buffered with $NaHCO_3$ (1.0 mmol/L, pH 8.5) respectively. The generation of ROS/RNS standard solutions were given in Supporting information. To test the specificity of this assay, various ROS/RNS were also tested separately using the same procedures as that of BPO. The detail detecting process were also listed in Supporting information.

The prepared Au nanostructure were characterized by means of TEM, UV–vis absorption and Raman spectrum. As shown in TEM images (Fig. 1), the diameters and morphologies of both the MPBA-AuNPs$_{65}$ and the DPA-AuNPs$_{12}$ show little changes comparing with theirs precursors (Fig. S1). The physical mixture of the MPBA-AuNPs$_{65}$ and the DPA-AuNPs$_{12}$ in deionized water are dispersed separately without any crosslinking (Fig. 1C). After buffering under pH 8.5, they tended to assembly into core/satellite nanostructure (the BE-AuNPs$_{12/65}$) by forming borate ester (Fig. 1D). The LSPR peaks of the DPA-AuNPs$_{12}$ and the MPBA-AuNPs$_{65}$ located at 523 nm and 545 nm respectively (Fig. 1E). The achieved BE-AuNPs$_{12/65}$ show two plasmonic modes, *i.e.,* a dominant radiant mode at 665 nm which indicates strong core-to-satellite coupling, and a nonradiant mode existed as a shoulder on the left flank of spectrum between 520 nm and 560 nm, but the particular LSPR of the BE-AuNPs$_{12/65}$ is completely different from that of the individual building blocks or the physical mixture of them. The SERS spectra of both the TA-AuNPs and DPA-AuNPs were fairly weak due to their small Raman scattering cross sections. However, SERS spectrum of the MPBA-AuNPs is very prominent, benefiting from the thiolated linkers with conjugated π-electrons of MPBA [24], which is dominated by the characteristic bands of C—C in-plane bending at 1001 cm^{-1}, C—H in-plane bending mode at 1016 cm^{-1}, C—C in-plane bending mode coupled with C—S stretching at 1074 cm^{-1}, the peak related to the in plane movement of the ring carbons at 1186 cm^{-1}, as well as the totally symmetric ring stretching at 1587 cm^{-1}, respectively. As for the BE-AuNPs$_{12/65}$, several spectral changes such as the red shift of the in plane movement of the ring carbons from 1186 cm^{-1} to 1170 cm^{-1}, and the phenyl ring breathing vibration coupled with C—S stretching mode shifted from 1074 cm^{-1} to 1080 cm^{-1} suggest the polarity of phenyl ring changes. But the most prominent change is the peak of 8a (1597 cm^{-1}), a totally symmetric mode of MPBA decrease, while a shoulder peak of 8b (1582 cm^{-1}), a non-totally symmetric 8b mode appear. This distinct change indicated that the symmetry of the MPBA on AuNPs was broken because of forming dopamine-MPBA borate ester upon binding with the DPA-AuNPs [25,26].

TEM results verified the BPO-triggered deboronation, due to the average numbers of the DPA-AuNPs$_{12}$ around the cores MPBA-AuNPs$_{65}$ decreased gradually with the increment of the BPO concentrations (Figs. 2A and B). As expected, addition of BPO triggers the absorbance of the BE-AuNPs$_{12/65}$ at 665 nm attenuate (Fig. 2C), indicating the disassembly of the BE-AuNPs$_{12/65}$. To understand clear reaction mechanism in this case, the characteristic vibrational alterations of the BE-AuNPs$_{12/65}$ upon adding BPO were analysis using Raman spectra. As shown in Fig. 3D, a distinct SERS spectrum of the BE-AuNPs$_{12/65}$ after reacting with BPO was obtained, *i.e.*, C–H out of plane bending stretching at 821 cm^{-1}, ring breathing at 1007 cm^{-1}, the in-plane ring breathing mode coupled with C—C, C—S stretching at 1080 cm^{-1}, C—H bending at 1169 cm^{-1}, C—O stretching at 1279 cm^{-1}, C—H scissoring at 1490 cm^{-1} as well as benzene stretching vibrations around 1600 cm^{-1}, which was consistent with SERS spectrum of 4-mercaptophenol absorbed on AuNPs [27,28]. All of these results represented important evidences on the mechanism of the sensing strategy, BPO with high oxidation capacity could efficiently and specifically trigger deboronation of the BE-AuNPs$_{12/65}$ nanoprobe bearing arylboronate, and then adding a hydroxide radical in the same position of benzene ring, which was in full compliance with previous reported results [8–10].

The specific deboronation induced SPR absorbance change of the BE-AuNPs$_{12/65}$ would subsequently afford a new ratio metric absorbance signal for detecting BPO. The absorbance changes were correlated quantitatively with the BPO using the ratiometric peak intensities at 665 nm and 545 nm A_{665}/A_{545}, a good linear relationship (r = 0.995) can be readily described using the linear equation: $A_{665}/A_{545} = 1.09 - kC_{BPO}$, ($C_{BPO}$ represents the concentration of BPO, nmol/L), where the slope k acts as the aggregation constant

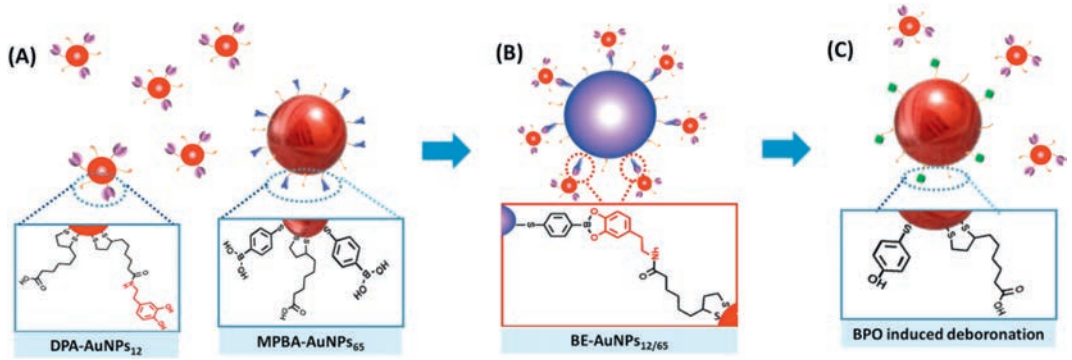

Scheme 1. Illustration of the general design of the core/satellite BE-AuNPs$_{12/65}$ and the sensing principle for BPO. (A) Modification of the larger AuNPs$_{65}$ and the smaller AuNPs$_{12}$ with MPBA and DPA ligands, respectively; (B) Conjugation of the satellite DPA-AuNPs$_{12}$ on the MPBA-AuNPs$_{65}$ by forming borate ester; (C) Disassembly of the BE-AuNPs$_{12/65}$ induced by BPO deboronation.

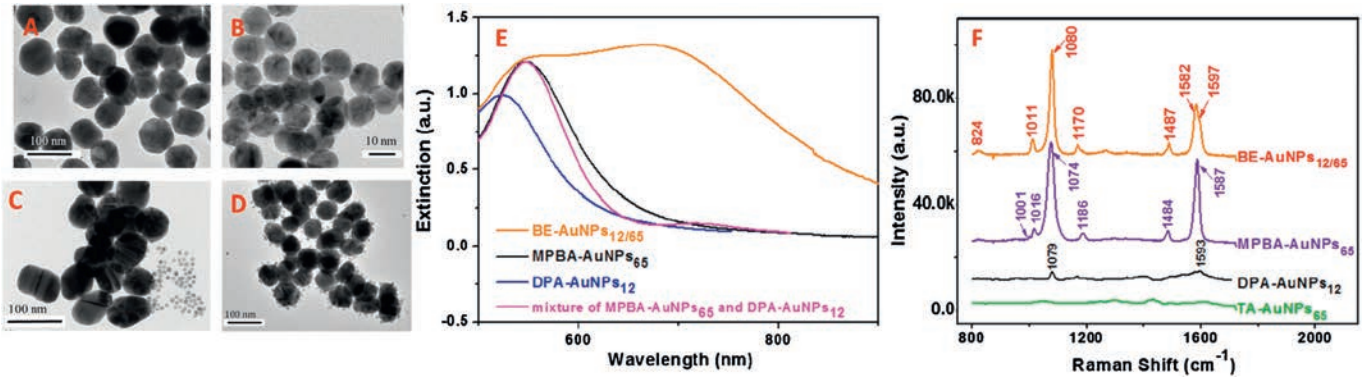

Fig. 1. TEM of (A) the MPBA-AuNPs$_{65}$, (B) the DPA-AuNPs$_{12}$, (C) the physical mixture of the MPBA-AuNPs$_{65}$ and the DPA-AuNPs$_{12}$ as well as (D) the resulting BE-AuNPs$_{12/65}$; Their respective UV–vis spectra (E) and the corresponding SERS spectra (F).

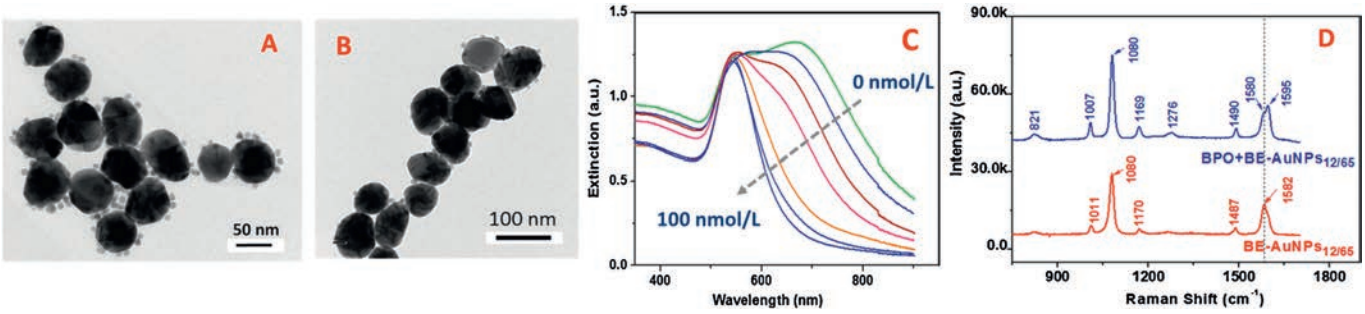

Fig. 2. TEM images the BE-AuNPs$_{12/65}$ under different BPO concentrations: 20 nmol/L (A), 100 nmol/L (B); UV–vis spectra (C) and the corresponding SERS spectra (D) of the BE-AuNPs$_{12/65}$ in the presence of BPO.

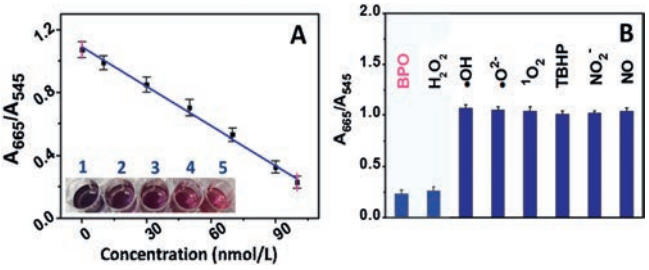

Fig. 3. (A) Color change of the BE-AuNPs$_{12/65}$ for different concentration of BPO from 1 to 5: 0, 20, 50, 70, 100 nmol/L (Inset photograph) and plot of A_{665}/A_{545} *vs.* concentration of BPO. (B) Selectivity of the BE-AuNPs$_{12/65}$ toward various RNS/ROS interferents at 10 μmol/L (Data are mean value of 3 measurements).

($k = 8.4 \times 10^{-3}$). The linear range of the method is 10–100 nmol/L, and the detection limit for BPO was determined to be approximately 7.2 nmol/L by including the control signal with three times of the standard deviation. The resulted A_{665}/A_{545} values gave a relative standard deviation (RSD) of 7.1% (50 nmol/L, $n = 6$), demonstrating satisfactory reproducibility of the proposed method. It was found that colorimetric response of the BE-AuNPs$_{12/65}$ to various possible coexisting substances (1.0 mmol/L) including Na^+, K^+, Mg^{2+}, Ca^{2+}, Cl^-, OAc^-, NO_2^-, NO_3^-, SO_3^{2-}, SO_4^{2-}, PO_4^{3-}, glycine, were negligible by monitoring the extinction ratio (A_{665}/A_{545}) under the same detecting conditions as BPO. Moreover, the response time of the proposed sensing system was examined. It was found that after reacting for 20 min, the absorbance of the BE-AuNPs$_{12/65}$ in the presence of BPO became stable. As indicated in Fig. 3, no obvious signal response of the BE-AuNPs$_{12/65}$ were observed when important ROS/RNS were added except H_2O_2, indicating the borate ester sensing interface provided it well selectivity for BPO. Considering that H_2O_2 could not be employed as food additive, it was less likely limiting the usefulness of the method.

Because the BPO is prohibited in flour as a food additive, developing sensitive on-field assay is of great significance in food safety fields. To examine practical applicability of the BE-AuNPs$_{12/65}$, BPO was firstly extracted from wheat-flour food samples (wheat flour, glutinous rice flour and noodle) using acetone (the detailed sample preparations were given in Supporting information), and then detected using the new developed AuNP nanoprobe. The extraction process could eliminate interfering substances such as glycogen, carbohydrate from real samples. As demonstrated in Table 1, the detecting results were suggesting the reliability of this new method in real application. Compared with other existing on field assays for BPO (Table S1 in Supporting information), this new proposed assay was

Table 1
Results for the determination of BPO in food samples.

Sample	BE-AuNPs$_{12/65}$ nanoprobe		Recovery (%)
	Spiked (nmol/L)	Detected (nmol/L)	
Wheat flour	0	ND[a]	–
	20	17.6	88.0
	50	45.7	91.4
Glutinous rice flour	0	ND	–
	20	18.1	90.5
	50	46.2	92.4
Noodle	0	ND	–
	20	17.2	86.0
	50	45.1	90.2

[a] Not detected.

not only of theoretical simplicity and low technical demands, but combined the advantages of simply, sensitive and accurate, which had well applicable potentials in rapid screening BPO.

In summary, a rapid and selective strategy was developed for the colorimetric detection of BPO at nanomolar levels. The homogeneous gold nanoprobe was fabricated based on the formation of borate ester between MPBA-AuNPs and DPA-AuNPs, which allowed for controlled nanoassembly, tailored plasmonic properties as well as specific sensing interface. Based on the specific deboronation of BPO, together with the well intrinsic plasmic properties of Au nanoassembly, a low-cost, and easy-to-use method was developed for sensitive and specific BPO screening in real food matrices.

Acknowledgments

The authors gratefully acknowledge financial support from the National Natural Science Foundation of China (Nos. U1736201, 21677019 and 41403021), Capital Health Research and Development of Special (No. 2018-4-1014) and the Key Research and Development Program of Beijing (No. D171100008317001).

Appendix A. Supplementary data

Supplementary material related to this article can be found, in the online version, at doi:https://doi.org/10.1016/j.cclet.2019.08.051.

References

[1] B.P. Lamsal, J.M. Faubion, LWT-Food Sci. Technol. 42 (2009) 1461–1467.
[2] W. Li, Q.N. Zhao, W.D. Song, J. Diseas. Monit. Control. 4 (2010) 391–392.
[3] G. Bhasin, H. Kauser, M. Athar, Arch. Toxicol. 78 (2004) 139–146.
[4] W. Chen, W. Shi, Z. Li, et al., Anal. Chim. Acta 708 (2011) 84–88.
[5] Z. Lei, Z. Zeng, X. Qian, Y. Yang, Chin. Chem. Lett. 28 (2017) 2001–2004.
[6] G. Mu, H. Liu, Y. Gao, F. Luan, J. Sci. Food Agric. 92 (2012) 960–964.
[7] Y. Abe-Onishi, C. Yomota, N. Sugimoto, H. Kubota, K. Tanamoto, J. Chromatogr. A 1040 (2004) 209–214.
[8] W. Chen, Z. Li, W. Shi, H. Ma, Chem. Commun. 48 (2012) 2809–2811.
[9] Y. Zhang, Y.Y. Fu, D.F. Zhu, et al., Chin. Chem. Lett. 27 (2016) 1429–1436.
[10] Q. Hu, W. Li, C. Qin, L. Zeng, J.T. Hou, J. Agric. Food Chem. 66 (2018) 10913–10920.
[11] C.A. Mirkin, R.L. Letsinger, R.C. Mucic, J.J. Storhoff, Nature 382 (1996) 607–609.
[12] H. Jans, Q. Huo, Chem. Soc. Rev. 41 (2012) 2849–2866.
[13] R.P. Holler, M. Dulle, S. Thoma, et al., ACS Nano 10 (2016) 5740–5750.
[14] J.H. Yoon, J. Lim, S. Yoon, ACS Nano 6 (2012) 7199–7208.
[15] Y. Zhao, X. Yang, H. Li, et al., Chem. Commun. 51 (2015) 16908–16911.
[16] L. Wang, L. Li, H.L. Ma, H. Wang, Chin. Chem. Lett. 24 (2013) 351–358.
[17] T. Lin, M. Zhang, F. Xu, et al., Sens. Actuators B-Chem. 261 (2018) 379–384.
[18] J. Sun, R. Liu, J. Tang, et al., ACS Appl. Mater. Interfaces 7 (2015) 16730–16737.
[19] X.D. Xia, H.W. Huang, Chin. Chem. Lett. 25 (2014) 1271–1274.
[20] H. Chen, Y. Xia, Anal. Chem. 86 (2014) 11062–11069.
[21] J. Duan, Z.Y. Guo, Chin. Chem. Lett. 23 (2012) 225–228.
[22] L. Lu, Y. Xia, Anal. Chem. 87 (2015) 8584–8591.
[23] N.G. Bastus, J. Comenge, V. Puntes, Langmuir 27 (2011) 11098–11105.
[24] F. Sun, T. Bai, L. Zhang, et al., Anal. Chem. 86 (2014) 2387–2394.
[25] P. Shen, Y. Xia, Anal. Chem. 86 (2014) 5323–5329.
[26] G. Springsteen, B.H. Wang, Tetrahedron 58 (2002) 5291–5300.
[27] R. Li, W. Ji, L. Chen, et al., Spectrochim. Acta Part A 122 (2014) 698–703.
[28] B.L. Scott, K.T. Carron, J. Phys. Chem. C 120 (2016) 20905–20913.